Effect of chaos in a one-channel time-reversal acoustic mirror

Alejo Alberti,[1] Diego A. Wisniacki,[2] Gaston Maffei,[2] and Manuel C. Eguia[1,*]
[1]*Laboratorio de Acústica y Percepción Sonora, Universidad Nacional de Quilmes, R. S. Peña 352, Bernal, (1875) Buenos Aires, Argentina*
[2]*Departamento de Física and IFIBA, FCEN, Universidad de Buenos Aires, Ciudad Universitaria, Pab. I (1428) Buenos Aires, Argentina*

(Received 15 January 2019; published 12 July 2019)

Time-reversal of propagating waves has been intensely studied during the last years and successfully implemented in different experimental contexts. It has been argued that ergodic or chaotic ray dynamics improve the refocusing resolution. In this work we consider this fundamental aspect by studying the reversion of sound waves in two-dimensional reflecting cavities numerically. The boundary of the enclosure is deformed from a rectangle with regular ray dynamics to a completely chaotic hyperbolic billiard. We observed that both the regular and chaotic cases display a prominent refocusing peak, and also that in the first scenario many secondary maxima appear. We developed measures of the spatial and temporal contrasts of the reconstructed signal in order to gain insight on these phenomena and to distinguish between cases. The results obtained point to the necessity for a reconsideration of what is usually understood by successful time-reversal processes.

DOI: 10.1103/PhysRevE.100.012208

I. INTRODUCTION

Time-reversal of waves is reported frequently in literature nowadays. This phenomenon started being studied in the 1990s with the pioneering work of Fink and his group [1]. Usually called "time-reversal mirror", it is a technique that allows for the focusing of a signal onto a narrow region in space by emitting a time-reversed version of the received wave field measured by an array of transducers. This procedure has been successfully accomplished in acoustic [2], elastic [3,4], and electromagnetic waves [5] in different setups, and several applications based on it have been found [6–8]. The refocusing property is due to the linear reciprocity of the wave equation.

When the reversion is performed in a closed cavity and without absorption, the presence of many transducers to record and replicate the original signal is not needed. In fact, it has been shown that the reversion is very good with only one channel [3] though with certain theoretical limitations for the refocusing of the energy [10]. That is, the injection of a single pulse in a cavity yields a signal in another point. By recording and reversing a part of this signal, a sharp peak is obtained at the injection point. But in this case the need of underlying chaotic ray dynamics has been stressed as a fundamental factor for obtaining a good reversion [9,10]. Although this was mentioned in several works in the literature, as far as we know, there has yet not been a systematic study on the influence of chaos on the temporal reversion. For example, in Ref. [9] a semi-classical study of time-reversal focusing was developed for chaotic cavities but the integrable case was only referred mentioned to stress that the refocusing depends strongly on the position of the transducers. Nevertheless, as can be deduced from results in Ref. [11], the behavior of ray dynamics seems not to have any influence on the quality of the focusing. Therefore, a study that clears doubts about the influence of chaos on reversion is important and necessary. We note that the connection between classical chaos and wave mechanics has been greatly studied in the context of quantum mechanics, giving rise to quantum chaology or quantum chaos. Many wave manifestations of ray chaos were well established as the connection of the statistical spectral distributions and the Random Matrix Theory [12].

The goal of this paper is to study the effect of chaos in the one-channel reversion of acoustic waves in two-dimensional cavities. For this reason we consider a cavity without dissipation as a model system. Closed cavities are paradigmatic systems in classical dynamics, the shape of their boundaries determining the type of dynamics they develop. For example, rectangle billiards are completely regular, while chaotic dynamics are developed when one of the walls is curved. We studied the time-reversal acoustic mirror in a one-parameter family of billiards that displays the transition from integrable to chaotic ray dynamics. While the expected refocusing resulting from the time-reversal process is observed in every case, for the regular geometries a number of secondary maxima appear. This effect was detected through inspection of the resulting fields.

In order to quantify the quality of the reversion the temporal and spatial contrasts are commonly employed, which measure, respectively, the degree of focusing at the reversion time or at the injection point, and which can be written as functions of the eigenmodes and eigenfrequencies of the cavity. Remarkably, while the effect of underlying chaotic ray dynamics is detected on the spatial contrast, the same is not true for the temporal contrast. An explanation for this phenomenon is provided, based on the modal content of each type of system. Moreover, in the literature the usual definitions of contrast employed [10,11] are based on RMS values, and as a consequence the quantitative influence of the reported secondary peaks is averaged out. Therefore, in this work we introduce new definitions of spatial and temporal contrasts to

*Corresponding author: meguia@unq.edu.ar

take account of such features. These new definitions can also be used to hint the chaoticity of a system. We also provide an explanation for the origin of such maxima, based on the method of images.

The paper is organized as follows. In Sec. II we present the main theoretical aspects of the time-reversal mirror and we define the two measures of temporal and spatial contrasts which can be written as functions of the eigenmodes and eigenfrequencies of the cavity. Section III is devoted to describe the systems under study: a family of perturbed two-dimensional rectangular cavities with ray dynamics that range from regular to completely chaotic. We describe the numerical procedures employed to obtain the eigenmodes and eigenfrequencies of the cavities. In Sec. IV we show the results produced by a systematic study of the different measures of contrast in several cavities. We consider the dependence of these measures on the size of the time window applied to filter out the part of the signal to revert, and on the cutoff frequency employed in the calculation of the eigenfrequencies of the system. We also consider the dependence of the spatial contrast on the perturbation parameter that quantifies the deviation of the chaotic geometries from the regular systems. We end the paper with some final remarks on the topic of time-reversal mirrors.

II. TIME-REVERSAL MIRROR AND CONTRAST

A. Time-reversed signal

Let us suppose that at time $t = 0$ a sharp perturbation is produced in $\mathbf{r} = \mathbf{r_A}$. The time evolution of this perturbation in a two-dimensional medium is described by the nonhomogeneous wave equation

$$\Big(\frac{1}{c^2}\frac{\partial^2}{\partial t^2} - \nabla^2\Big)\phi(\mathbf{r}, t) = F\delta(\mathbf{r} - \mathbf{r_A})\delta(t),$$

where c is the wave speed and F is the amplitude of the perturbation. The time evolution can be expanded in the eigenmodes $\phi_i(\mathbf{r})$ of the cavity, $\phi(\mathbf{r}, t) = \sum a_i(t)\phi_i(\mathbf{r})$ with $a_n(t) = Fc^2\cos(\omega_n t)$ and ω_i the corresponding eigenfrequency. The possibility of expanding the solution in these terms will be useful for what follows.

When we consider the case of single-channel time reversion, a stimulus $f(t)$ (with $t \in [0, T]$) is emitted at point $\mathbf{r_A}$ and recorded at point $\mathbf{r_B}$. Then, a part of the recorded signal $v(t)$ is reversed in time and re-emitted from $\mathbf{r_B}$. We are interested in observing the resulting signal at $\mathbf{r_A}$. As is well known, a tool for characterizing the transfer function of a system between two points is the impulse response (IR) [13]. The IR represents the response of a system when stimulated by a pulse, which mathematically can be noted as a δ function. As the Fourier expansion of such a stimulus is comprised of all possible excitation frequencies, the stimulation produced by a pulse contains information about the stimulation with any single frequency, and the full transfer function of the system can actually be computed as the Fourier transform of the IR.

Being $h_{AB}(t)$ the impulse response from $\mathbf{r_A}$ to $\mathbf{r_B}$ we can write

$$v(t) = \int_{-\infty}^{\infty} f(t')h_{AB}(t - t')\,dt' \tag{1}$$

If the stimulus $f(t)$ employed is actually the impulse response (IR) itself, cut from $t = T_1$ to $t = T_2$ and inverted in time, then it can be written as

$$f(t) = \begin{cases} h_{AB}(T - t) & \text{if } t \in [T - T_2, T - T_1] \\ 0 & \text{if } t \notin [T - T_2, T - T_1] \end{cases}.$$

The time-reversal process is completed after emitting this signal from $\mathbf{r_B}$ and observing the result in $\mathbf{r_A}$. By virtue of the symmetry of the impulse response h_{AB} with respect to the pair of points $(\mathbf{r_A}, \mathbf{r_B})$ the resulting signal in $\mathbf{r_A}$, v_{TR}, can be computed inserting the defined f in Eq. (1). Naming $\Delta_{T_2,T_1} = [T - T_2, T - T_1]$, it turns out to be

$$v_{TR}(t) = \begin{cases} 0 & \text{if } t < T - T_2 \\ \int_{T-T_2}^{t} h_{AB}(T - t')\,h_{AB}(t - t')\,dt' & \text{if } t \in \Delta_{T_2,T_1} \\ \int_{T-T_2}^{T-T_1} h_{AB}(T - t')\,h_{AB}(t - t')\,dt' & \text{if } t > T - T_1 \end{cases}. \tag{2}$$

Note that regardless of the choice for T_1, T_2, v_{TR} attains its maximum value at $t = T$, where the integral is equal to the autocorrelation function of h_{AB}. This corresponds with observing the maximum of the re-emitted signal at the refocusing time.

For $t < T - T_2$ the signal observed at $\mathbf{r_A}$ is null, since the re-emitted recording, starting at $T - T_2$, displays no information there. For the case $t \in \Delta_{T_2,T_1}$ we can find expressions for T_{mn} in terms of known quantities by making use of a Fourier expansion. As can be shown [10,11], the impulse response h_{AB} can be written as a summation over eigenmodes. With ϕ_i the acoustic fields of the system corresponding to eigenfrequencies ω_i, it is seen that

$$h_{AB}(T - t') = \sum_m \phi_m(\mathbf{r_A})\phi_m(\mathbf{r_B})\cos(\omega_m(T - t')),$$
$$h_{AB}(t - t') = \sum_n \phi_n(\mathbf{r_A})\phi_n(\mathbf{r_B})\cos(\omega_n(t - t')).$$

By inserting these series in Eq. (2) v_{TR} takes the form

$$v_{TR}(t) = \sum_{m,n} \phi_m(\mathbf{r_A})\phi_n(\mathbf{r_A})\phi_m(\mathbf{r_B})\phi_n(\mathbf{r_B}) \times \underbrace{\int_{T-T_2}^{t} \cos(\omega_m(T - t'))\cos(\omega_n(t - t'))\,dt'}_{T_{mn}(t)}. \tag{3}$$

Depending on the complexity of the geometry, the eigenmodes ϕ_i can be computed either by analytical or numerical procedures. We now focus on finding a closed expression for the matrix T_{mn} in terms of the eigenfrequencies and of the time window limits T_1, T_2. Beginning with a change of variables

$$d = t - T$$
$$s = T - t',\ ds = -dt',$$

T_{mn} can be written as

$$\begin{aligned} T_{mn}(t) &= -\int_{T_2}^{T-t} \cos(\omega_m s)\cos(\omega_n(s+d))\,ds \\ &= \cos(\omega_n d)\int_{-d}^{T_2} \cos(\omega_m s)\cos(\omega_n s)\,ds \\ &\quad - \sin(\omega_n d)\int_{-d}^{T_2} \cos(\omega_m s)\sin(\omega_n s)\,ds. \end{aligned}$$

Using basic trigonometrical properties and defining

$$\omega_+ = \omega_m + \omega_n$$
$$\omega_- = \omega_m - \omega_n,$$

the former expression for T_{mn} can be seen to reduce to

$$\begin{aligned} T_{mn}(t) = \frac{\cos(\omega_n d)}{2}&\left[\frac{\sin(\omega_+ T_2)+\sin(\omega_+ d)}{\omega_+}\right. \\ &\left.+\frac{\sin(\omega_- T_2)+\sin(\omega_- d)}{\omega_-}\right] \\ +\frac{\sin(\omega_n d)}{2}&\left[\frac{\cos(\omega_+ T_2)-\cos(\omega_+ d)}{\omega_+}\right. \\ &\left.-\frac{\cos(\omega_- T_2)-\cos(\omega_- d)}{\omega_-}\right]. \end{aligned}$$

On the other hand, for the case $t > T - T_1$ changing the superior limit of integration ($t \to T - T_1$, which implies $-d \to T_1$) and following an analogous procedure leads to

$$\begin{aligned} T_{mn}(t) = \frac{\cos(\omega_n d)}{2}&\left[\frac{\sin(\omega_+ T_2)-\sin(\omega_+ T_1)}{\omega_+}\right. \\ &\left.+\frac{\sin(\omega_- T_2)-\sin(\omega_- T_1)}{\omega_-}\right] \\ +\frac{\sin(\omega_n d)}{2}&\left[\frac{\cos(\omega_+ T_2)-\cos(\omega_+ T_1)}{\omega_+}\right. \\ &\left.-\frac{\cos(\omega_- T_2)-\cos(\omega_- T_1)}{\omega_-}\right]. \end{aligned}$$

The time dependency of the results is in the variable $d = t - T$.

Equation (3), with the corresponding expression depending on the value of t, defines the time dependence of the observed field at $\mathbf{r_A}$ after the time-reversal process, in terms of the modal behavior of the cavity. In particular, note that the modal fields $\phi_i(x)$ are evaluated at the locations $\mathbf{r_A}$ and $\mathbf{r_B}$. This implies that the time-reversal is better between points at which the same modal fields display maxima, i.e., at points located symmetrically with respect to some axis of symmetry of the cavity, should such an axis exist.

B. Temporal and spatial contrasts

When the time-reversal of a given signal takes place, an important concentration of energy can be found at the location $\mathbf{r_A}$ of the original source at the refocusing time T. This gives rise to two main quantities that can be computed to determine the quality of the time-reversal process for a given cavity.

The first quantity is the spatial contrast. In the literature [11] it is usually defined as the ratio between the wave amplitude at $\mathbf{r} = \mathbf{r_A}$ and the root mean square of the wave amplitudes in every other point of the cavity, at the reversion time:

$$C_s^{\mathrm{RMS}} = \frac{|v_{TR}(\mathbf{r_A}, T)|}{\sqrt{\langle v_{TR}^2(\mathbf{r} \neq \mathbf{r_A}, T)\rangle}}. \tag{4}$$

It can be noted that this definition does not provide information on the existence of secondary maxima which may compete in importance with the one that arises from the refocusing at the original source location. For reasons that will be clear later on, it is useful to introduce an additional definition of spatial contrast, which takes that possibility into account, allowing to distinguish between different scenarios. Considering that the quality of the time-reversal process does not only depend on the formation of an outstanding localized spatial maximum but that it also implies the uniqueness of that maximum, an alternative definition is based on the comparison between the maximum at $\mathbf{r} = \mathbf{r_A}$ and the maximum wave amplitude at any other point:

$$C_s^{\max} = \frac{|v_{TR}(\mathbf{r_A}, T)|}{\max|v_{TR}(\mathbf{x}, T)|} \tag{5}$$

with $\mathbf{x} : ||\mathbf{x} - \mathbf{r_A}|| > l$ so as to discard points that belong to the region surrounding the maximum at $\mathbf{r_A}$, where a resonance with characteristic width l takes place. The idea is that if the peak arising from the refocusing is prominent with respect to the background noise, and that it also is unique, then C_s^{RMS} together with $C_s^{\max}$ would point that fact out.

The other quantity of interest is the temporal contrast. Following the previous observations we will again consider two definitions, one based on an RMS average

$$C_t^{\mathrm{RMS}} = \frac{|v_{TR}(\mathbf{r_A}, T)|}{\sqrt{\langle v_{TR}^2(\mathbf{r_A}, t \neq T)\rangle}} \tag{6}$$

and another on the comparison between maxima

$$C_t^{\max} = \frac{|v_{TR}(\mathbf{r_A}, T)|}{\max|v_{TR}(\mathbf{r_A}, t \neq T)|}. \tag{7}$$

Taking into account expression (3) it can be seen that the contrasts to be calculated depend on the cutoff frequency considered for the computation of the eigenfrequencies. Also, as previously stated, the signal received at $\mathbf{r_B}$ is cut from $t = T_1$ to $t = T_2$ before conducting the reversion. Two parameters are then defined for characterizing the resulting signal: the cutoff frequency f_{cut} and the width $w = T_2 - T_1$ of the time window employed.

III. NUMERICAL MODELS

As we are interested in studying the behavior of the time-reversal process throughout the transition from a regular system to a chaotic one, we consider an air-filled acoustical rectangular cavity with non-commensurable sides ($L_x = \pi$, $L_y = 2$, in meters) and a family of perturbed cavities, replacing two adjacent walls with circumference arcs with contact angle θ, while keeping the same area $R = 2\pi$ m^2. The case $\theta = 0$ corresponds to the regular system and the chaoticity is increased

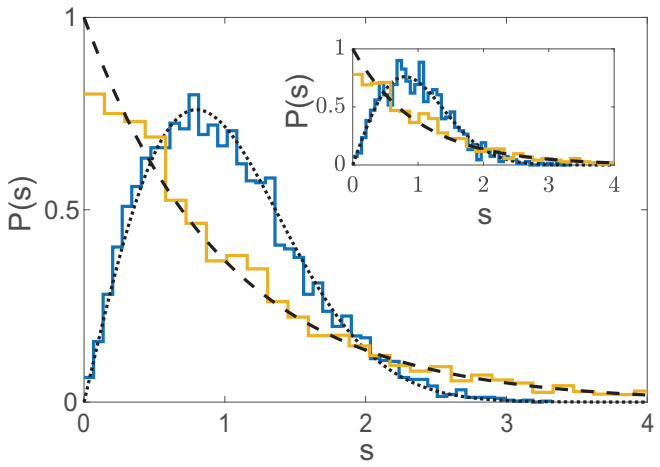

FIG. 1. Nearest-neighbor distribution $P(s)$ of the first 6000 eigenfrequencies for the geometries under study. In orange we display the behavior for the non-degenerated (with non-commensurable sides) rectangular cavity, which is correctly described by a Poissonian distribution $P_P(s)$, drawn in black dashed line. The corresponding distribution for the perturbed cavity ($\theta = 20$) is pictured in blue, and we superimpose a Wigner-Dyson $P_{WD}(s)$ curve in black dots for reference. Both reference curves (Poisson and Wigner) were obtained from the numerical results for the eigenfrequencies, and confirm the underlying level distribution (regular, chaotic) for each type of system. In the inset the same distributions are shown but considering only the first 1000 eigenlevels. The clear qualitative differences are seen to persist under this lower spectral regime.

with θ. A commensurable rectangle case was also considered. The sides of this rectangle were $L_x = 2, L_y = 3\,\mathrm{m}$, giving rise to modal degeneration. The qualitative behavior for this system was found to be very similar to the corresponding one for the non-commensurable rectangle, in terms of spatial and temporal contrasts. Hence, from now on this case will not be mentioned.

The first step to compute the spatial and temporal contrasts was to obtain the eigenmodes of the cavities, from the analytic solutions for $\theta = 0$ and through a finite element method (FEM) commercial software implementation (COMSOL Multiphysics [14]) for $\theta \neq 0$. For each case, the first $\approx$6000 eigenfrequencies and eigenfunctions were computed. All the calculations were repeated using different grid sizes to check for numerical convergence of the FEM.

As a tool for determining the chaoticity arising from the different geometries we computed the nearest-neighbor distribution $P(s)$ of the eigenfrequencies for the two cavities. This is shown in Fig. 1. The distribution $P(s)$ shows a clear indication of the regular-chaotic transition: levels of systems with integrable ray dynamics can cross and the distribution is Poissonian, $P_P(s) = \exp(-s)$, (s is the normalized level spacing) while crossings are avoided in chaotic systems and the level spacing distribution is given by the Wigner-Dyson distribution, as predicted by random matrix theory $P_{WD}(s) = (\pi s/2)\exp(-\pi s^2/4)$ [15]. We also checked that the spectral distribution of the eigenfrequencies follows Weyl's law [16].

An additional study consisted of inspecting the level spacing distribution for different superior cut-off frequencies. In particular, the distributions were also observed considering only the first 1000 (see inset in Fig. 1), 2000, 3000, 4000, 5000 eigenfrequencies, verifying that the qualitative differences between the rectangular and deformed cavities still hold, and that the Poissonian and Wigner-Dyson distributions, respectively, still provide proper fits. This allows to state that the different geometries give rise to integrable or chaotic ray dynamics under various spectral regimes (in particular, under all those that will be considered henceforth).

After obtaining the modal components, ω_i, and the corresponding acoustic fields in all space, ϕ_i, we used Eq. (3) to compute the theoretical time-reversed signal to be observed when the reversion is conducted between points $\mathbf{r_A}$ and $\mathbf{r_B}$. This procedure was repeated for all the systems.

For the computation of the spatial contrast for each geometry 30 different pairs of random points were considered, in order to obtain statistical results which average out the behavior of ill-conditioned points. For the dependence against f_{cut} we considered values between 900 and 5900 Hz, in steps of 500 Hz. For the dependence against w, on the other hand, we considered time windows with widths ranging from 10 to 980 ms, always centered at $T/2 = 500$ ms.

The calculations for temporal contrast were carried out taking 1000 random $\mathbf{r_A}$, $\mathbf{r_B}$ pairs of points for each geometry, and the ranges for f_{cut} and w were the same as before.

IV. RESULTS

Let us consider the case of a time-reversal process involving a source placed in $\mathbf{r_A}$ and a recording position $\mathbf{r_B}$. The emitted signal is recorded during a time window of width w, then reversed in time and re-emitted (in every possible direction) from $\mathbf{r_B}$. As a first result we display in Fig. 2 the time-reversed signal as recorded at the position of the original source ($\mathbf{r_A}$) for the two configurations. In the figure we also show the acoustic field in all the space at the reversal time, which is taken as $t = 0$ for convenience.

In panels (a,b) of Fig. 2 the recorded signals at point $\mathbf{r_A} = (x_A, y_A)$ exhibit a sharp peak for both systems. This occurs at the refocusing time, when the original signal is reconstructed at the position of the original source due to the convergence of multiple wave-fronts in phase. The corresponding fields are shown in panels (b, d). In both cases it is found that the amplitude of the temporal as well as of the spatial peaks are very similar. Also, calculations on the spatial distributions of energy show that the relation between the energy of the main peak corresponds to approximately 1/3 times the energy of the whole field, consistently with the theoretical predictions [10]. No significant differences are observed in that ratio when considering the different geometries.

For the rectangular geometry a remarkable feature is observed. In addition to the amplitude maximum at $\mathbf{r_A}$ a number of secondary maxima arise. Two secondary maxima with an amplitude close to one-half that of the main peak are found aligned at the same x_A coordinate as the principal maximum, and the same happens along the y_A coordinate. Additional maxima are found aligned with these secondary peaks displaying an amplitude about 1/4 that of the main reversed peak. In contrast, the chaotic system does not exhibit secondary peaks.

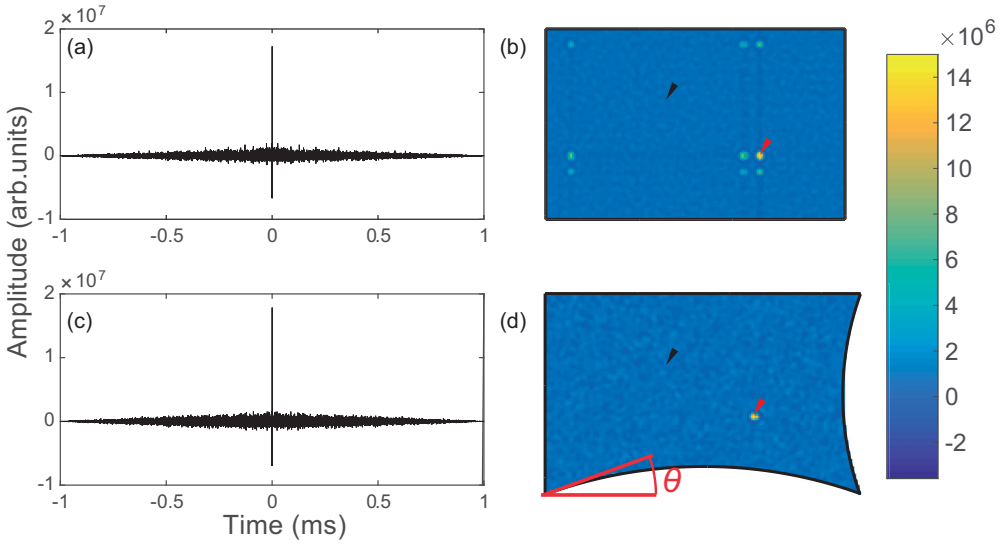

FIG. 2. (a) Time dependence of the reversed signal at the position where the pulse was originally emitted $\mathbf{r_A}$, for a rectangular acoustical cavity with $L_x = \pi$ and $L_y = 2$ m. The origin of time was chosen so that the refocusing occurs at time $T = 0$. (b) The corresponding wave field at the refocusing time. The positions of the original source $\mathbf{r_A}$ and the receptor $\mathbf{r_B}$ are pointed with red and black arrows, respectively. In (c) and (d) the corresponding time reversed signal and wave field at the refocusing time are displayed for the chaotic cavity with $\theta = 20$. At all instances the area with fixed at 2π m^2.

From these representations it is clear that the introduction of the definition of spatial contrast given by Eq. (5) is necessary to account for these effects.

The presence of secondary maxima for the rectangular cavity can be explained using the method of images. Let $\mathbf{r_A^{k,l}}$ and $\mathbf{r_B^{m,n}}$ be the multiple images corresponding to the original emitting and recording points, indexed in the (x, y) cavity images by the integers pairs (k, l) and (m, n), respectively. The impulse response from $\mathbf{r_A}$ to $\mathbf{r_B}$ can be determined by calculating the acoustical paths $\Lambda^{k,l} = \mid \mathbf{r_A^{k,l}} - \mathbf{r_B} \mid$. Since during reversal all the images $\mathbf{r_B^{m,n}}$ act as sources, coincident wavefronts will occur at point $\mathbf{r}$ whenever $\Lambda^{k,l} = \mid \mathbf{r_B^{n,m}} - \mathbf{r} \mid$ for multiple (k, l, m, n) quadruplets. In this scenario, the main refocusing at $\mathbf{r} = \mathbf{r_A}$ corresponds to an infinite number of coincident wavefronts obtained making $k = \pm m$ and $l = \pm n$, with the plus (minus) sign for odd (even) integers.

In Fig. 3 we illustrate, as an example, the acoustical paths from four images of the original source to the recording position, and the wavefronts from the images of the recording position (that act as re-emission points) with radii equal to the corresponding acoustical paths lengths. The four wavefronts are coincident at the location of the original source.

In order to find the secondary maxima we reduce the problem to the easily solvable one-dimensional case of a cavity of length L. In Table I we display four acoustical paths (x_A^{-1} to x_A^{+2}) as columns and two images x_B^0 and x_B^{-1} as rows. Each path is added and subtracted from the image coordinate, since during time-reversal each image emits two pulses (moving towards positive and negative directions) for each recorded pulse. All higher order acoustical paths and images give coordinates that overlap with those displayed in Table I which, when restricted to the interval $[0, L]$, lead to only three refocusing points: the original source point x_A and two secondary maxima C and D. The coordinates of these secondary maxima depend on the relative position of x_A and x_B, as follows:

$$C\begin{cases} x_B < x_A/2 & \boxed{C_1} \\ x_B \geqslant x_A/2 \ \wedge \ x_B \leqslant (x_A + L)/2 & \boxed{C_2} \\ x_B > (x_A + L)/2 & \boxed{C_3} \end{cases}, \tag{8}$$

$$D\begin{cases} L - x_B < x_A/2 & \boxed{D_1} \\ L - x_B \geqslant x_A/2 \ \wedge \ L - x_1 \leqslant (x_A + L)/2 & \boxed{D_2} \\ L - x_B > (x_A + L)/2 & \boxed{D_3} \end{cases}. \tag{9}$$

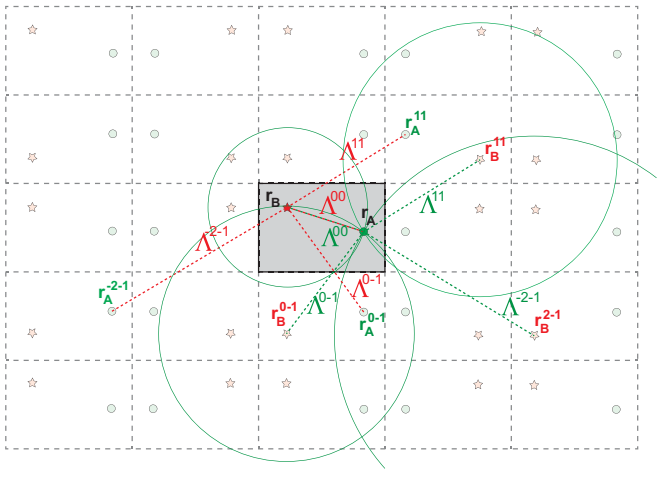

FIG. 3. An illustration of the image method for finding time-reversed focusing points. The acoustical paths from each of four images of the original source ($\mathbf{r_A^{0,0}}$, $\mathbf{r_A^{0,-1}}$, $\mathbf{r_A^{1,1}}$, and $\mathbf{r_A^{-2,1}}$) to the recording position $\mathbf{r_B}$ are displayed as red dotted segments. The corresponding wavefronts with the same radii, re-emitted from four images of the recording position ($\mathbf{r_B^{0,0}}$, $\mathbf{r_B^{0,-1}}$, $\mathbf{r_B^{1,1}}$, and $\mathbf{r_B^{2,-1}}$) are displayed in green dotted line and overlap at the original source location $\mathbf{r_A}$.

TABLE I. Locations where the convergence of wavefronts occur at the reversal time. Some of them lie within the cavity (in particular, x_A) and some others outside, independently of the locations (x_A, x_B). Some others, marked with letters, may or not be in $[0, L]$ depending on the relation between x_A and x_B, see Eqs. (8) and (9). The table can be extended infinitely in both directions, but the remaining virtual images will produce wavefronts always outside the cavity.

Image \ Distance	$x_A^{-1} = x_A + x_B$	$x_A^0 = x_A - x_B$	$x_A^1 = 2L - x_B - x_A$	$x_A^2 = 2L - x_B + x_A$
x_B+	$2x_B + x_A$ D_3	x_A	$> L$	$> L$
x_B-	<0	$2x_B - x_A$ C_2	$-2(L - x_B) + x_A$ D_1	<0
$-x_B+$	x_A	$x_A - 2x_B$ C_1	$2(L - x_B) - x_A$ D_2	$2(L - x_B) + x_A$ C_3

The locations of the secondary maxima C and D can also be obtained by reflecting x_A with respect to x_B and $(L - x_B)$, respectively, and taking its images if the result lies outside the interval $[0, L]$. This solution generalizes to the two-dimensional case as longitudinal modes in the x and y directions. In fact the secondary maxima are obtained by reflecting $\mathbf{r_A}$ with respect to the lines $x = x_B$, $x = L_x - x_B$, $y = y_B$, and $y = L_y - y_B$, and taking its images if needed. Therefore a Cartesian product of the solution of the one-dimensional case, is also a solution for the two-dimensional case, giving nine focusing points.

As discussed before,the spatial and temporal contrasts can be studied in terms of their dependence on the type of underlying geometry, and also as functions of the defined quantities f_{cut} (cutoff frequency) and w (time window). In Fig. 4 we display the spatial contrasts [using both definitions (4) and (5)] as functions of those quantities for the geometries under study.

Taking panel (a) into consideration, the first observation is that the spatial contrast grows with the cutoff frequency. The positive dependence is reasonable because more eigenmodes are considered for the reconstruction of the signal as f_{cut} grows, and hence more wavefronts interfere constructively at the position of the original source at the reversal time.

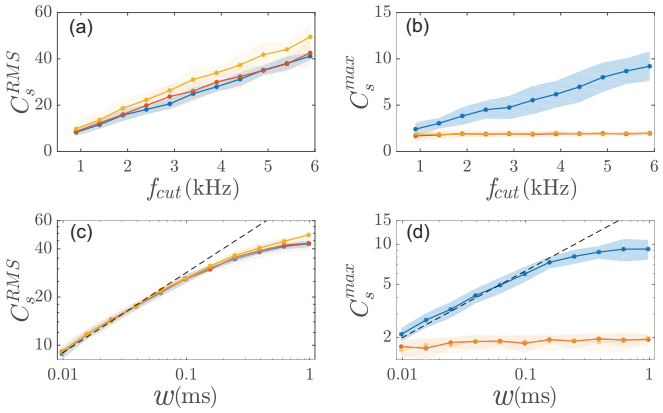

FIG. 4. Spatial contrasts as functions of f_{cut} (a,b) and w (c,d). In (a,c) the averaging definition given by Eq. (4) is employed, and in (b,d) the one given by Eq. (5). The curves in the panels correspond to the average results for deformed (blue) and regular (orange) rectangles, and are displayed together with their corresponding standard deviations. A linear projection is also presented in dashed black line.

A similar reasoning can be developed to explain (c), where it is seen that the contrast grows with the widening of the time window. In this case it seems evident that as w grows the signal to be reversed contains more energy, as it is the equivalent of taking a larger portion of the original emission. Both behaviors seem to be roughly the same for the two systems when definition (4) is employed. Also it is noticed that while the contrast grows roughly linearly throughout the whole range of values of f_{cut} considered, is seems to saturate for values of w near 0.75 ms, where a plateau is attained.

On the other hand some remarkable features are observed when considering panels (b) and (d). It is noted that the curve for the deformed rectangle (in blue line) clearly departs from the one corresponding to the regular geometry (in orange line), indicating that the definition of contrast based on comparisons between maxima (5) allows for the identification of each type of system. For the rectangular case that measure is equal to the ratio between the amplitudes of the main and secondary peaks, which is approximately equal to 2. For the deformed geometry, however, the behavior is similar to the one observed in panels (a), (c)—where the averaging definition erases the influence of such maxima—since there are no secondary maxima.

In Fig. 5 we display the results for the temporal contrast for each system, again as functions of the cut-off frequency and f_{cut} and the time window employed for the reversal w.

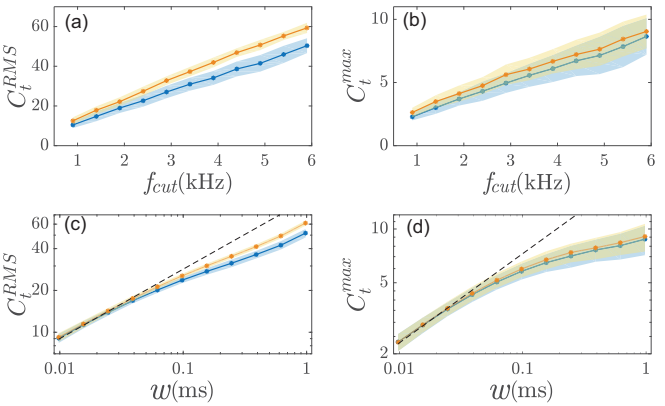

FIG. 5. Temporal contrasts as functions of f_{cut} (a,b) and w (c,d), as given by Eqs. (6) and (7). The curves in the panels correspond to the average results for deformed (blue) and regular (orange) rectangles, and are displayed together with their corresponding standard deviations. A linear projection is also presented in dashed black line.

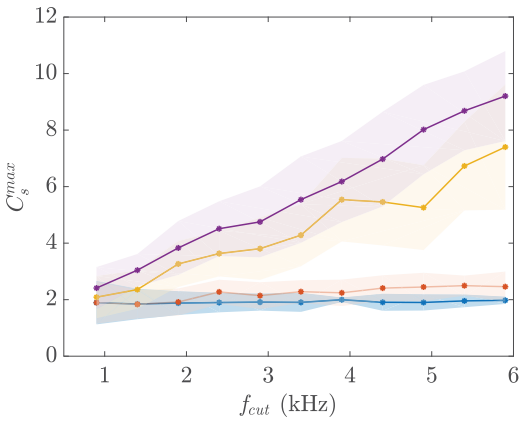

FIG. 6. Spatial contrasts as functions of f_{cut}, as given by Eq. (5). Each curve corresponds to values of θ of 0 (blue), 1 (red), 5 (yellow), and 20 (violet) degrees. The behavior of the contrast changes remarkably for a value of θ between 1 and 5 degrees. As in Fig. 4, the values of contrast were averaged over 30 pairs of random points and in this picture we display those results together with the corresponding standard deviations.

In this case it is interesting to see that both geometries seem to display similar behaviors, using both definitions and considering the dependence on both parameters. The temporal contrast again grows linearly with f_{cut} and suggests some saturation as w is increased approaching 1 ms, especially under the second definition of contrast. The most important result here is that the temporal contrast is not affected significantly by the chaotic dynamics as compared to those of regular type, and also that both definitions of contrast lead to the same conclusions.

This feature can be understood in terms of the mechanism leading to the formation of the refocused peak, as follows. First, it is important to notice that when the initial acoustical excitation is applied the various wavefronts produced arrive to the receiving location coming from specific directions (depending on the reflections they experienced on the surrounding walls), but, on the contrary, the emission of the reversed signal is performed in every direction simultaneously, as a cylindrical or spherical excitation. As discussed for the one-dimensional (1D) scenario some of the wavefronts emitted in different directions can interfere constructively after several reflections, giving rise to secondary maxima; the same reasoning can be applied to cases with more dimensions. It is therefore reasonable to conclude that increasing the number of eigenfrequencies considered for the excitation, as well as widening the time window employed to cut the signal, results in stronger convergences at the refocused maximum, therefore enhancing the spatial contrast. For the temporal contrast, however, the phenomenology is different: the formation of secondary maxima at the reversal location implies the existence of periodic components in the temporal reversion, which result in maxima localized in time when overlapped. These periodic components are series of commensurable frequencies, and need to have a relatively important weight on the spectrum in order to have a noticeable effect as a whole. This condition is always met for the 1D case because all the eigenfrequencies are integer multiples, giving rise to a periodic signal as a result of the reversal. On the other hand, for the two-dimensional (2D) scenario there are also sequences of eigenfrequencies which are integer related, such as those defined by the separations between parallel walls ('bouncing ball' modes). If the total amount of eigenfrequencies considered for the excitation signal is moderate then those modes which are in a sequence can be relatively important globally. But as the cut-off frequency increases, the number of elements in the periodic series grows linearly, while the total amount grows quadratically (according to Weyl's law) and as a result the relative weight of the modes that belong to a periodic series approaches zero as $\sim 1/f$. In that case no recurrence is observed on the reversed signal, and in sum the temporal contrast does not experience considerable fluctuations due to the geometry of the system under study. This is precisely what is observed on the numerical results. We can therefore conclude that the differences between the behaviours of the temporal and spatial contrasts originate on the non-preservation of the directions of arrival for the reversed wavefronts.

As a final study we calculated the spatial contrast (5) for different values of perturbation angle θ (see Fig. 6). This provided insight on the quantitative relevance of the chaotic dynamics for the enhancement of the contrast. We considered values of θ between 0 and 20 [corresponding to non-commensurable and deformed rectangles, respectively, see panels (b) and (d) in Fig. 2] finding that a clear difference in the contrast curves occurs for a value of θ between 1 and 5 degrees.

V. CONCLUSIONS

The influence of chaotic dynamics on the quality of time-reversal processes was argued for in the literature. To our notice, however, no work had so far been developed to demonstrate such necessity. In this paper we developed systematic studies on regular and chaotic systems in an attempt to determine how fundamental the underlying dynamics are for the adequate conduction of the time-reversal process. We used measures of spatial and temporal contrast as quantities to gauge the quality of the results.

The numerical computations carried out showed that for every geometry considered the refocusing effect manifests, leading to a prominent peak in the amplitude of the field. It was also manifest that there are no significant differences on the prominence of that peak among the different geometries. By inspection of the time-reversed fields, however, we observed that the conduction of the time-reversal process on regular geometries leads to the manifestation of some relevant secondary peaks. We provided an explanation for their origin, locations and relative amplitudes by means of the method of images.

In quantitative terms, when the usual definition for contrast (as the ratio between the energy of the main peak and the energy of background noise) is employed there are no important differences on the resulting values for the different geometries. This suggests that, under this definition, chaos actually is not a requisite for a good quality time-reversal. To take account of the appearance of the secondary peaks we proposed a new definition for contrast, as the ratio between

the energies of the most important peak and of the subsequent maximum. Under that definition there is a clear difference on the behaviours of the regular and chaotic systems. Considering regular geometries with and without modal degeneration allowed us to confirm that the differences arise from the chaoticity of the systems, and not from the separation of eigenfrequencies alone.

As mentioned, it was shown that a number (eight) of secondary maxima appear when the time-reversal process is performed on the rectangular cavities. These maxima are clearly noticeable and carry $1/4$ or $1/16$ times as much energy as the main reversal peak. In spite of that, the ratio of energy of the peak against the RMS value of the energy of the background throws a value close to the theoretical limit maximum of $1/3$. This fact confirms the relevance of the additional definition of contrast proposed in this work, that sheds further light on the underlying behavior of the system by pointing out the existence of secondary maxima.

When considering the temporal contrast no noticeable differences were found using either of the definitions of contrast involved in this work. This is again remarkable, especially considering the differences in spatial contrast. An explanation for this feature was provided here, based on the underlying mechanisms leading to secondary maxima both in the spatial and in the temporal aspects of the reverted signal.

It must be kept in mind that the proposed contrast measure does not suffice by itself to determine whether a system is chaotic or not, although it actually helps on signaling the possible existence of chaos. From the performed simulations chaos was shown to be related to the non existence of secondary time reversal maxima. Also, this measurement is not necessarily the only possible one to hint for this type of behavior. In fact under some circumstances, using short reconstruction times and a limited number of high frequency modes, noticeable differences appear with respect to the usual measurement of contrast, although this can not be widely generalized to other scenarios. As an advantage, the differences on the measurement of contrast comparing with secondary maxima (the newly introduced definition) are observed for every reconstruction time and number of modes, both in higher and lower frequencies, as was shown in the presented figures. Other measures, for example based on the stability of the reconstructed signal against perturbations, can be further explored.

The results shown here, together with those previously reported in the literature, point to the need for a reconsideration of what is defined as a successful time-reversal process. Given the linear reciprocity of the wave equation, the underlying physics allows for the reversion at all instances. However, as was shown here, a unique refocused peak occurs only under some particular circumstances (chaotic dynamics), while the time-reversal process gives rise to many maxima otherwise (regular dynamics). If a good reversion is considered to occur whenever some focusing is found at the original source location, then there are no clear differences arising from the underlying dynamics. If, on the other hand, a good-quality reversion is said to occur whenever that condition is met together with the uniqueness of that maximum, then only chaotic systems allow for the phenomenon, and the newly introduced definition of spatial contrast is necessary to distinguish between scenarios.

ACKNOWLEDGMENTS

The authors would like to thank R. Jalabert and H. Pastawski for their useful discussions. The authors have received funding from CONICET Grant No. PIP-11220150100493CO, PUNQ Grant No. 1394/2015, UBACyT Grant No. 20020170100234BA, and ANCyPT Grant No. PICT-2016-1056.

[1] M. Fink, Phys. Today **50**(3), 34 (1997).
[2] A. Derode, P. Roux, and M. Fink, Phys. Rev. Lett. **75**, 4206 (1995); M. Fink, Phys. Scr. T **90**, 268 (2001).
[3] C. Draeger and M. Fink, Phys. Rev. Lett. **79**, 407 (1997).
[4] S. Catheline, N. Benech, J. Brum, and C. Negreira, Phys. Rev. Lett. **100**, 064301 (2008).
[5] G. Lerosey, J. deRosny, A. Tourin, A. Derode, G. Montaldo, and M. Fink, Phys. Rev. Lett. **92**, 193904 (2004).
[6] M. Fink, G. Montaldo, and M. Tanter, Annu. Rev. Biomed. Eng. **5**, 465 (2003).
[7] B. T. Taddese, J. Hart, T. M. Antonsen, E. Ott, and S. M. Anlage, Appl. Phys. Lett. **95**, 114103 (2009).
[8] M. Frazier, B. Taddese, Th. Antonsen, and S. M. Anlage, Phys. Rev. Lett. **110**, 063902 (2013).
[9] H. L. Calvo, R. A. Jalabert, and H. M. Pastawski, Phys. Rev. Lett. **101**, 240403 (2008).
[10] C. Draeger and M. Fink, J. Acoust. Soc. Am. **105**, 618 (1999).
[11] Ch. Hudin, J. Lozada, and V. Hayward, J. Sound Vib **333**, 1818 (2014).
[12] H.-J. Stöckmann, *Quantum Chaos: An Introduction* (Cambridge University Press, Cambridge, 2000).
[13] H. Kuttruff, *Room Acoustics* (Spon Press, New York, 2009).
[14] COMSOL Multiphysics Reference Manual, version 5.3, COMSOL, Inc, www.comsol.com.
[15] O. Bohigas, M. J. Giannoni, and C. Schmit, Phys. Rev. Lett. **52**, 14 (1984).
[16] H. Primack and U. Smilansky, Phys. Rep. **327**, 1 (2000).